

NUMERICAL SIMULATION OF LIQUID HYDROGEN EVAPORATION IN THE PRESSURIZED TANK DURING VENTING

Kangwanpongpan, T., Makarov, D., Cirrone, D. and Molkov, V.

HySAFER Centre, Ulster University, Jordanstown, Shore Road, Newtownabbey, BT37 0QB, UK

Corresponding author: T.Kangwanpongpan@ulster.ac.uk

ABSTRACT

CFD modelling of liquified hydrogen boiling and evaporation during the pressurised tank venting is presented. The model is based on the volume-of-fluid method for tracking liquid and gas phases, and Lee's model for phase change. The simulation results are compared against the liquid hydrogen evaporation experiment performed by Tani et al. (2021) in a large-scale pressurised storage tank, using experimental pressure dynamics and temperatures measured in gas and liquid phases. The study focuses on tank pressure decrease and recovery phenomena during the first 15 s of the venting process. The model sensitivity have been studied applying different Lee's model evaporation-condensation coefficients. The CFD model provided reasonable agreement with the observed pressure and gas phase temperature dynamics during the liquid hydrogen storage depressurisation, using Lee's model coefficient $r = 0.05 \text{ s}^{-1}$. Experimentalists' hypothesis about particularly intensive boiling in the proximity of thermocouples was supported by close agreement between simulated and experimental saturation temperatures obtained from pressure dynamics.

1.0 INTRODUCTION

Perspective heavy-duty hydrogen applications are likely to utilize liquified hydrogen (LH2), causing interest in the safety of LH2 handling, storage and fuelling. Though the computational models describing multiphase flows – phase tracking, boiling, condensation – are available and developed, their applications for predicting LH2 behaviour are still lacking comprehensive validation and clarification of the model parameters for typical industrial processes. An analysis of the typical modelling approaches, available and used for simulation of LH2 boiling and evaporation, is presented below.

A large body of LH2 boiling and evaporation studies in engineering context exercised the equilibrium modelling approach, i.e. equal velocities and temperatures of liquid and gas phases, in combination with the volume-of-fluid (VOF) [1] method for phase tracking and Lee's model [2] for the simulations of evaporation and condensation problems [3-11]. However, the simulated physical setup and accordingly the set of model parameters were significantly different between the authors.

Kim et al. [3] studied the phase change in thermosyphon. The constant Lee's model evaporation coefficient value 0.1 s^{-1} was applied, while the condensation coefficient was a function of liquid density to a gas density ratio. Filling of LH2 in storage tank was simulated by Ma et al. [4], where Lee's model coefficient values between 0.01 s^{-1} and 100 s^{-1} were tested. Finally, the coefficient value 0.1 s^{-1} was found to provide the best agreement in comparison with the experimental data.

Thermal stratification in LH2 propellant tank, filled at 32% LH2 by volume and having size 3.3 m radius and 11.3 m height, was modelled by Liu et al. [5] under variable gravity conditions. The Lee's model coefficient of 0.1 s^{-1} was used for the description of both evaporation and condensation.

LH2 pressurisation, hold and expulsion were investigated via numerical simulations by Li et al. [6] following experiment performed by NASA [12]. The LH2 spherical storage tank was 1.52 m in diameter and was filled at 95% level. The best agreement to the experimental measurements was found using Lee's model coefficient value 6.0 s^{-1} .

Exposure of a 0.8 m diameter storage tank to 800 W/m^2 heat flux leading to LH2 self-pressurization was studied by Zhou et al. [7]. The tested evaporation and condensation coefficients were in the range $0.05 - 0.2 \text{ s}^{-1}$ and it was found that the value 0.2 s^{-1} fitted the experimental observations best.

Lv et al. [8] studied the effect of gravity and tank geometry on the LH2 pressurization rate with tank filled up to 90% of storage level. The evaporation coefficient values varied in between 10^{-4} and 10^{-5} s^{-1} , though the condensation coefficient was kept constant at 10^4 s^{-1} . The authors concluded that the evaporation coefficient of 10^{-5} s^{-1} provided a good match to the experimental observations.

Flashing cryogenic liquid under rapid depressurisation was studied by Watanabe et al. [13] using liquified nitrogen. The authors investigated the transient phenomena of pressure recovery, i.e. pressure decreased below the initial pressure and then increased due to flashing evaporation, using different rates of venting. It was observed that the larger venting and depressurisation rates resulted in a more pronounced pressure recovery - deeper pressure drop followed by a stronger pressure peak (though not reaching the initial pressure value). Similar pressure recovery phenomena but for liquified hydrogen were studied experimentally and using CFD analysis by Tani et al. first in [9] and then in [10]. Much faster pressure rise was observed in the simulation results compared to the experimental dynamics, which was attributed to the absent hydrogen condensation in the CFD model, as its effect was initially thought to be negligible.

To the best of authors' knowledge, no special treatment of turbulence is used in the CFD simulations of multiphase flows in safety engineering context, including cryogenic gases and liquids. Kassemi and Kartuzova [11] studied an impact of turbulent models on pressure dynamics in the pressurised cryogenic hydrogen storage tank. Laminar flow model and turbulent modelling approach, using Reynolds-averaged Navier-Stokes (RANS) equations with the two-equations $k-\omega$ SST turbulence model, were applied. The finding was that the turbulent flow model resulted in a significant underprediction of vapour temperature in tank ullage. Molkov et al. [14] published the study and influence of applying laminar, standard $k-\epsilon$ and dynamic large-eddy simulation (LES) Smagorinsky-Lilly [15] model on the simulation of sub-sonic release and dispersion of helium in an enclosure. The best agreement, between experimental data on helium concentrations and the simulation results, was obtained when the LES turbulent model was applied.

The present study describes a CFD model to predict liquid and gas phases' behaviour in a pressurised LH2 storage tank with a focus on the initial stage of the flash-boiling process. This is one of the most challenging problems in the context of CFD numerical prediction of liquid and gaseous hydrogen evaporation due to depressurisation and venting. The simulated results for pressure, temperature and liquid level are presented in the resulting section 5 of this paper.

2.0 THEORETICAL METHOD

2.1 Governing equations

The CFD model included three-dimensional compressible mass, momentum and energy conservation equations, presuming equilibrium between liquid and gas phases (i.e. equal velocities and temperatures of LH2 and GH2 phases). Turbulence was modelled using LES approach with sub-grid scale Smagorinsky-Lilly model [15]; following the conclusion of the study [14]. It is expected that the LES approach will be able to seamlessly blend simulations of laminar, transitional and mildly turbulent flow regimes, which is expected to occur in different fluid flow regions during evaporation-condensation process, starting from the initially quiescent condition in gaseous and liquid phases.

2.2 Volume-of-fluid method

Volume-of-fluid (VOF) method [1] has been used for tracking phase change between liquid and gas phases. Solution of continuity equation for the gaseous phase was used in the CFD model presenting in this paper, in which the volume fraction for the liquid phase is determined from total sum of unity between these two phases. The source term in mass conservation equation and VOF transport equation is determined by the mass transfer between gaseous and liquid phases, also contributed to the source term in energy conservation equation.

The continuity equation for volume fraction of gaseous phase is solved as follows:

$$\frac{\partial(\alpha_G \rho_G)}{\partial t} + \nabla \cdot (\alpha_G \rho_G \vec{v}_G) = (\dot{m}_e - \dot{m}_c), \quad (1)$$

where \dot{m}_e and \dot{m}_c are the mass transfer rates due to evaporation and condensation respectively (kg/s-m^3), α_L and α_G are the volume fractions of liquid and gaseous phases (-), ρ_G is the density of gaseous phase (kg/m^3), t is time (s), \vec{v} is velocity vector (m/s). The volume fraction of liquid phase is determined from the identity:

$$\alpha_G + \alpha_L = 1. \quad (2)$$

The energy source term $S_{energy} = -\dot{m}_{transfer} L_{heat}$ accounts for the energy generated or absorbed by the phase change, where $\dot{m}_{transfer} = (\dot{m}_e - \dot{m}_c)$ is the mass transfer rate between phases, and L_{heat} is the latent heat of vaporization. The energy source becomes the heat source or sink depending on the phase change dominated by either evaporation or condensation. Thus, the energy source is negative for evaporation and positive for condensation. The latent heat is determined from the gas and liquid phase enthalpies for GH2 and LH2 [16] as:

$$L_{heat} = (h_G^s - h_L^s), \quad (3)$$

where the saturation enthalpies h_G^s and h_L^s are determined by the reference enthalpies plus the integral of the specific heat capacities over the change of saturation temperature from the reference value. The saturation enthalpies are:

$$h_G^s = h_G^{ref} + \int_{T_{ref,G}}^{T_{sat}} C_{p,G} dT \quad \text{and} \quad h_L^s = h_L^{ref} + \int_{T_{ref,L}}^{T_{sat}} C_{p,L} dT, \quad (4)$$

where $T_{ref,G}$ and $T_{ref,L}$ are the reference temperatures for GH2 and LH2 (K), T_{sat} is the saturation temperature (K), h_G^{ref} and h_L^{ref} are the reference enthalpies for GH2 and LH2 (J/kg), $C_{p,G}$ and $C_{p,L}$ are the specific heat capacities of GH2 and LH2 phases respectively (J/kg-K). In this study the reference temperature was chosen as the saturation temperature at 1 bar, $T_{ref,G} = T_{ref,L} = 20.3$ K.

In the VOF method, the temperature is shared between the phases and energy E is defined as:

$$E = \frac{\alpha_L \rho_L E_L + \alpha_G \rho_G E_G}{\alpha_L \rho_L + \alpha_G \rho_G}, \quad (5)$$

where the energy terms E_L and E_G for each phase are in the form $E_L = h_L - \frac{p}{\rho_L} + \frac{v^2}{2}$ and $E_G = h_G - \frac{p}{\rho_G} + \frac{v^2}{2}$ (J/kg), where ρ_L and ρ_G are the densities of liquid and gaseous phases respectively (kg/m^3), h_L and h_G are the enthalpies of gaseous and liquid phases, p is pressure (Pa) and v is velocity (m/s).

2.3 Phase change model

The Lee's model for evaporation and condensation is used [2] in this study. The mass transfer rate is described depending on the liquid and gas temperature as presented below.

For evaporation ($T_L > T_{sat}$):

$$\dot{m}_e = r_e \alpha_L \rho_L \frac{(T_L - T_{sat})}{T_{sat}}, \quad (6)$$

and for condensation ($T_G < T_{sat}$):

$$\dot{m}_c = r_c \alpha_G \rho_G \frac{(T_{sat} - T_G)}{T_{sat}}, \quad (7)$$

where \dot{m}_e and \dot{m}_c are the mass transfer rates due to evaporation and condensation (kg/s-m^3), r_e and r_c are the coefficients for Lee's model (s^{-1}) that are defined by the inverse problem method to match the experimental data, T_L and T_G are the temperatures of liquid and gaseous phases (K).

2.4 GH2 and LH2 properties

Real gas equation of state (EoS) by Peng-Robinson [17] is used to determine the density of GH2 phase. Density of LH2 phase was modelled depending on temperature, assuming that LH2 is at a saturation state. The polynomial function for LH2 density, dependent on temperature in a saturation stage, is fitted against NIST database [18] in the pressure range $(1.0 - 6.0) \cdot 10^5$ Pa presented as:

$$\rho_L = 73.168 + 0.8712 T - 0.0484 T^2. \quad (8)$$

For multiphase flow model, the model requires an information on the saturation temperatures varying with pressures (“ P ”) in the range $(1.0 - 6.0) \cdot 10^5$ Pa [18] and can be approximated via polynomial function as:

$$T_{sat} = 17.1 + (3.797 \times 10^{-5}) P - (5.198 \times 10^{-11}) P^2 + (3.3 \times 10^{-17}) P^3. \quad (9)$$

In the CFD model, the real gas specific heat capacity, $C_{p,G}$, is calculated as a sum of ideal gas specific heat, $C_{p,G}^0$, and a correction term, which depends on the used real gas EoS. The ideal gas specific heat capacity $C_{p,G}^0$ is obtained from the data published by Leachman et al. [19] and approximated as:

$$C_{p,G}^0 = 10,950 - (40.3) T + (0.6641) T^2 - (0.00268) T^3 + (3.468 \times 10^{-6}) T^4. \quad (10)$$

Similar to the same assumption used to determine LH2 density, the specific heat capacity of liquid phase is equal to that at the saturation state, $C_{p,L,sat}$, based on the data by McCarty et al. [20], which is about 4% lower than data determined using NIST database. The polynomial function for $C_{p,L,sat}$ is described by the polynomial function of temperature as:

$$C_{p,L,sat} = 10,563 - 645.59 T + 29.466 T^2. \quad (11)$$

The latent heat of hydrogen evaporation is calculated as $L_{heat} = (h_G^s - h_L^s)$ presented in Eq.(3). The reference temperatures for GH2 and LH2 are set to be equal to the saturation temperatures at 1 bar, $T_{ref} = 20.3$ K. Reference enthalpy for GH2 is set to the latent heat of vaporization at reference temperature, $h_G^{ref} = 448,917$ J/kg [18].

3.0 VALIDATION EXPERIMENT

Hydrogen flashing experiment by Tani et al. [9] has been used in this study employing CFD simulations. The experiment was conducted at JAXA Noshiro Rocket Testing Center and the LH2 tank had total volume 30 m^3 , height 7.622 m and internal diameter 2.3 m. The LH2 level was at height of 6.248 m from the bottom of the tank and initial pressure inside the tank at the start of experiment was 321,800 Pa (gauge).

Altogether 16 thermocouples were located along a thermometer probe in the tank: 4 probes denoted as TIE01-TIE04 in the gaseous hydrogen (GH2) area and 12 probes denoted as TIE05-TIE16 in LH2 zone (with TIE05 near the LH2 surface and TIE16 near the tank bottom). In this study the simulated temperatures are compared against all 4 probes in the ullage area (TIE01-TIE04), and 4 probes in LH2 zone (TIE05, TIE06, TIE07 and TIE08).

The experimentally measured mass flow rate at vent pipe was used as CFD boundary condition, see Fig. 1a. Dynamics of experimental pressure recovery shown in Fig. 1b was measured in the vent pipe during the first period of 15 s of release. The reproduction of the pressure obtained from the CFD simulations against this experimental pressure recovery is the primary research focus in this paper.

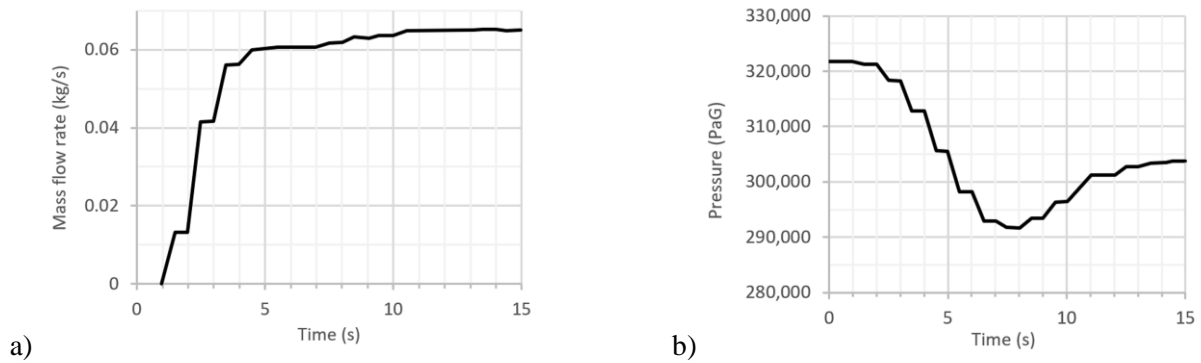


Figure 1. a) Mass flow rate during the first 15 s. b) Pressure recovery dynamics in the vent pipe.

4.0 CFD MODEL

4.1 Calculation domain and numerical mesh

The calculation domain was created to reproduce the LH2 tank geometry and presented in Fig. 2a. The domain was meshed using hexahedral control volumes (CV) and the total CV number is 251,272. The experimental paper didn't contain an information about the location and depth of protrusion of the vent pipe, therefore in the CFD model the pipe is positioned along the centre-line with the pipe entrance located at 6.672 m height (0.95 m below tank ceiling). The experimentally measured mass flow rate presented in Fig. 1a is used as an input into the CFD model.

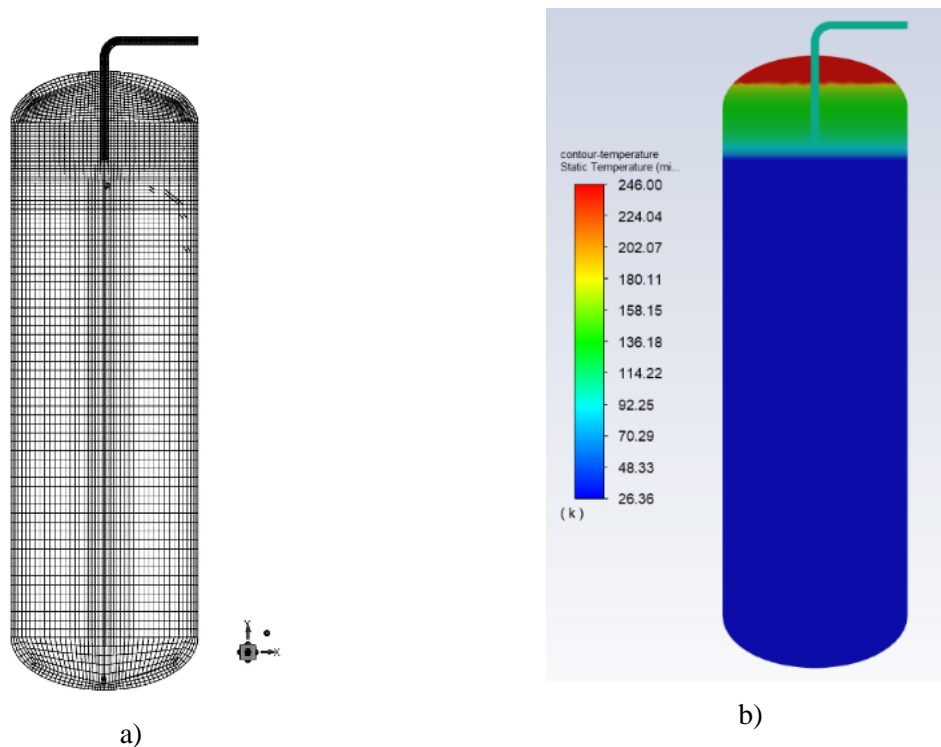


Figure 2. a) Calculation domain and the numerical mesh, central cross-section, b) Initial temperature distribution

4.2 Initial and boundary conditions

At the initial moment, $t = 0$ s, both GH2 and LH2 phases are quiescent as presented in Fig. 8a. The volume fraction of LH2 is set equal to 1.0 up to the height of 6.248 m from tank bottom. The initial temperature distribution in GH2 phase in the ullage zone is set by utilising the experimental data, increasing from 26.36 K at the LH2 surface up to 245 K near the tank top as shown in Fig. 2b. It is

noted that the initial GH2 temperature at the pipe entrance was equal to 100 K, which is important as the GH2 volumetric flow rate depends on its density and thus temperature. The initial LH2 temperature is equal to the saturation temperature $T_{sat} = 26.36$ K at the initial gauge pressure $p = 321,800$ Pa. Hydrostatic pressure at the bottom of the tank at initial moment is around 1.3% higher than the gauge pressure in GH2 phase, which is quite small and shouldn't impact the saturated pressure value and simulation results.

The tank has one outlet boundary condition, set as the pressure outlet at the end of the vent pipe. To implement the mass flow control in the vent pipe, the velocity of GH2 in the pipe is set using the experimental mass flow rate as an input. The experimental report [9] didn't contain an information on the heat flux through the tank wall, thus the heat flux in the CFD model was obtained based on the experiment performed by NASA [21]. There the LH2 tank was insulated using multi-layer insulation (MLI) blanket and the vacuum jacket, resulting in the total heat flux of approximately 3.4 W/m². Therefore, in this CFD model, the constant heat flux 3.4 W/m² is set as a boundary condition for energy equation over the entire tank wall surface. Since there was no information on the pipe wall design and material in the experimental paper [9], the adiabatic boundary condition is set as a thermal boundary for the vent pipe's surface.

4.3 Numerical details

The model is implemented using ANSYS Fluent 2020R2 as an CFD engine. The pressure-based solver is used together with the coupled scheme for pressure-velocity coupling. The scheme allows the use of larger time step in transient simulations, while retaining numerical stability and convergence comparing to iterative SIMPLE scheme. The PRESTO discretization scheme for pressure is utilised. Second order upwind scheme is used for the discretization of density, momentum and energy equations. The Geo-Reconstruct scheme is used for the discretization of volume fraction. The explicit formulation for volume fraction in multi-phase model is utilised together with sharp interface modelling between LH2 and GH2 area. At the start of simulation, the timestep was set to 10^{-4} s and then gradually increased to 0.002 s. The hydrogen mass balance was monitored in simulations at every timestep, and the maximum mass imbalance was within 4×10^{-5} %.

5.0 CFD SIMULATION RESULTS

5.1 Pressure recovery in LH2 tank

Pressure recovery dynamics in the LH2 tank measured during first 15 s in the experiment [9] was used and compared with simulated pressure obtained from the CFD simulations in this study.

Figure 3 shows experimental and modelled pressure transients obtained using two values of Lee's model evaporation and condensation coefficients: $r_e = r_c = 0.05$ and $r_e = r_c = 0.1$. In the text below the evaporation and condensation coefficients will be referred as a single coefficient r , as in all simulations the value of evaporation coefficient was equal to the value of condensation coefficient.

Firstly, the evaporation and condensation coefficient $r_e = r_c = 0.1$ is selected for the simulation, referring to the literature review and the simulations performed in publications by several authors generally fitted to various types of problems [3-5]. It is significant to point out that Lee's model is based on a simplified saturation model for evaporation and condensation, therefore the optimum value of empirical coefficient r is still needed to be evaluated to be suitable for individually specific problem, depending on the conditions and specific phase change phenomenon in the observed experiment [22]. For this reason, another value of evaporation and condensation coefficient $r_e = r_c = 0.05$ is selected simply by using half of the value 0.1 from literature review, for further investigation of the influence on the prediction on pressure recovery profile through time, specifically for this LH2 flash-boiling problem in the tank during depressurisation. The selected value of $r_e = r_c = 0.05$ is also based on the first run of simulation when applying $r_e = r_c = 0.1$ and higher simulated value of minimum pressure level was investigated. Therefore, decreasing value of coefficient is expected to result in the difference pressure profile and possibility of an improvement for the reproduction of pressure recovery trend.

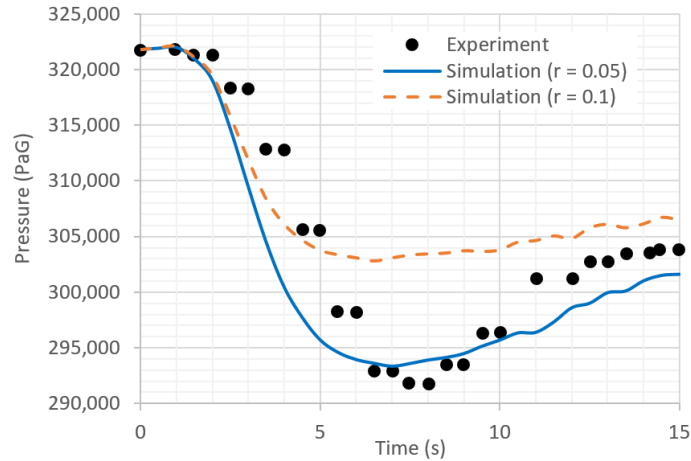


Figure 3. Experimental pressure recovery in LH2 tank comparing to simulated pressure dynamics using $r = 0.05$ and $r = 0.10$.

A better agreement with the experimental pressure dynamics is obtained when applying Lee's model coefficient $r=0.05 \text{ s}^{-1}$. Difference between experimental and simulated minimum overpressure is of the order 0.6% (measured overpressure is 292 kPa, simulated overpressure is 293.4 kPa), the difference between the same after pressure recovery is -0.7% (measured overpressure is 304 kPa and simulated one is 302 kPa, respectively). The pressure recovery in the simulations starts at 7 s while in the experiment it starts at about 7.5 s.

Lee's model coefficient $r=0.1$ resulted in an overestimation of the minimum pressure and a less pronounced pressure recovery. Thus, the experimental and simulated overpressures at their minimum were different by 3.8% (simulation overpressure is 303 kPa) and 1.0% after pressure recovery (simulated overpressure is 307 kPa), with the pressure recovery starting slightly earlier at 6.5 s. It is interesting that Lee's model coefficients $r=0.10$ was typically chosen by various authors in the past, while in this study the simulation results obtained with the coefficients $r = 0.05 \text{ s}^{-1}$ better fitted the experimentally observed pressure recovery.

5.2 GH2 phase temperature dynamics

Experimental and the simulated temperature dynamics in gaseous phase are compared along the positions of thermocouple probes TIE01-TIE04 in the ullage zone, located above the initial LH2 level as presented in Fig. 4. In the location of thermocouples TIE01-TIE03, the simulated temperature dynamics are in good qualitative agreements with the experimental records, even though the temperatures don't change much.

For the thermocouple TIE04, the simulated temperature starts to drop down much earlier than in the experiment – at 2.5 s, when the experimental temperature decreases at about 7.5 s. The simulated temperature reached as low as 28.5 K, which is close to the saturation temperature 26.36 K at experimental operating condition. The experimentalists suggested that when the LH2 level rises due to the flash-boiling, the TIE04 thermocouple probably submerges into boiling LH2, which could lead to the sharp drop of temperature as presented in Fig. 4 for TIE04. It is also interesting that the simulated temperature drops much smoother than in the experiment. The likely explanation of this observation is the absence of sharp phase transition between LH2 and GH2 in simulations using VOF method, where the "interface" in the CFD model is at least few control volume's wide. Yet the simulated TIE04 temperature at the end of 15 s period perfectly matches the experimental reading. In overall, the simulated temperatures in ullage zone (TIE01-TIE04) at time 15 s is quite accurate, in which the simulated temperatures depart from the experimental values by 3%, 6%, 30% and 9% in locations of TIE01-TIE04 thermocouples, respectively.

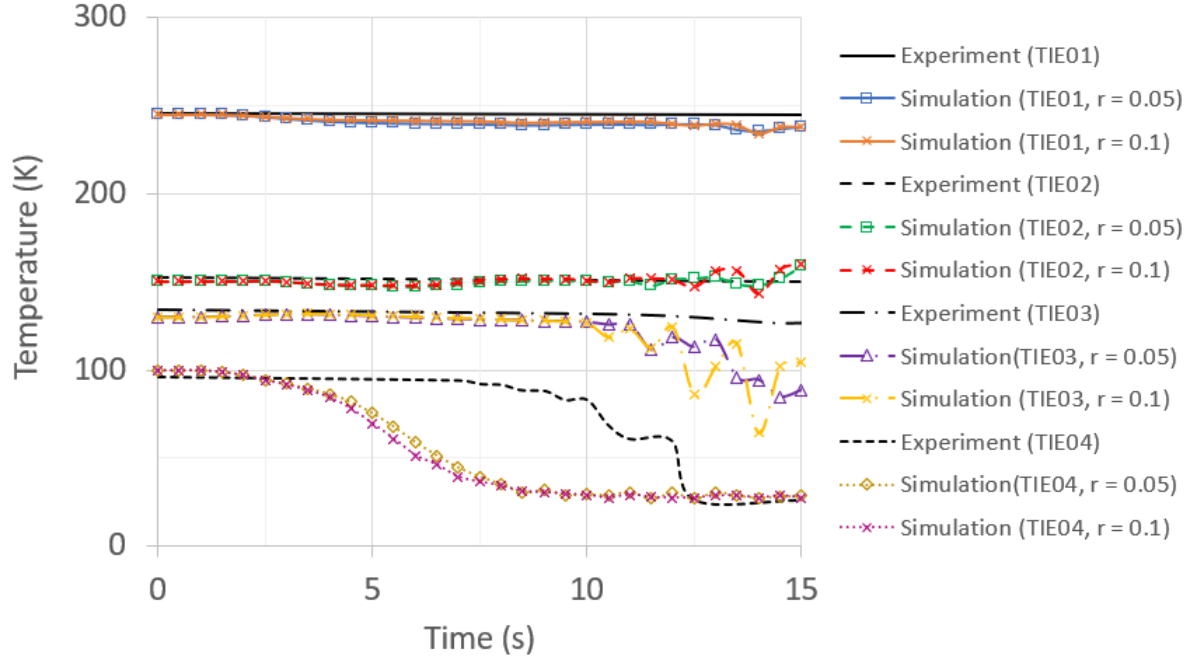


Figure 4. Experimental and simulated GH2 phase temperature dynamics, at probes TIE01-TIE04.

5.3 LH2 phase temperature dynamics

The simulated temperature dynamics in LH2 phase for Lee’s model coefficients $r=0.05$ is shown in Fig. 5 in location of thermocouples TIE05-TIE08 in comparison with the experimental records.

Initial temperature value in the position of thermocouple TIE05 (height of 6.222 m, located under the initial LH2 level at 6.248 m) is equal to the experimental value, 26.25 K as demonstrated in Fig. 5 (top left). The experimental record shows that the temperature decreased to 25.8 K at 6 s, followed by its recovery to 26.2 K at 15 s, which is not observed in the simulations – the simulated TIE05 temperature is quite steady varied within the temperature range 26.2-26.3 K. By the time $t = 15$ s, the experimental temperature recovers, and the difference between experimental and simulated temperatures diminishes.

The LH2 temperature drop was explained in the experimental report [9] to be occurred due to the intensive boiling around the thermocouples, which served as a heat sink in the thermocouple locations. The obtained simulation results may be used to inspect experimentalists’ hypothesis. Figure 5 shows the saturated temperatures T_{sat} , retrieved from simulation and from experimental pressure dynamics fitted to NIST database [18]. Now the simulated saturated temperature (marked “Simulation, T_{sat} ”) in TIE05 location closely follows the experimental saturated temperature determined using NIST database (marked “ $T_{sat, NIST}$ ”). It is noted that the saturated temperature, $T_{sat, NIST}$, is calculated by fitted the saturated temperatures of hydrogen to NIST database, in which saturated temperatures depend on experimental tank pressures through time. In simulations, the LH2 phase temperature is higher than the saturation one, meaning that the boiling process is ongoing, though not intensively enough to cause a measurable temperature decrease. At the same time, in the experiment, the saturation and the experimentally measured temperatures are close to each other, suggesting the intensive boiling occurred.

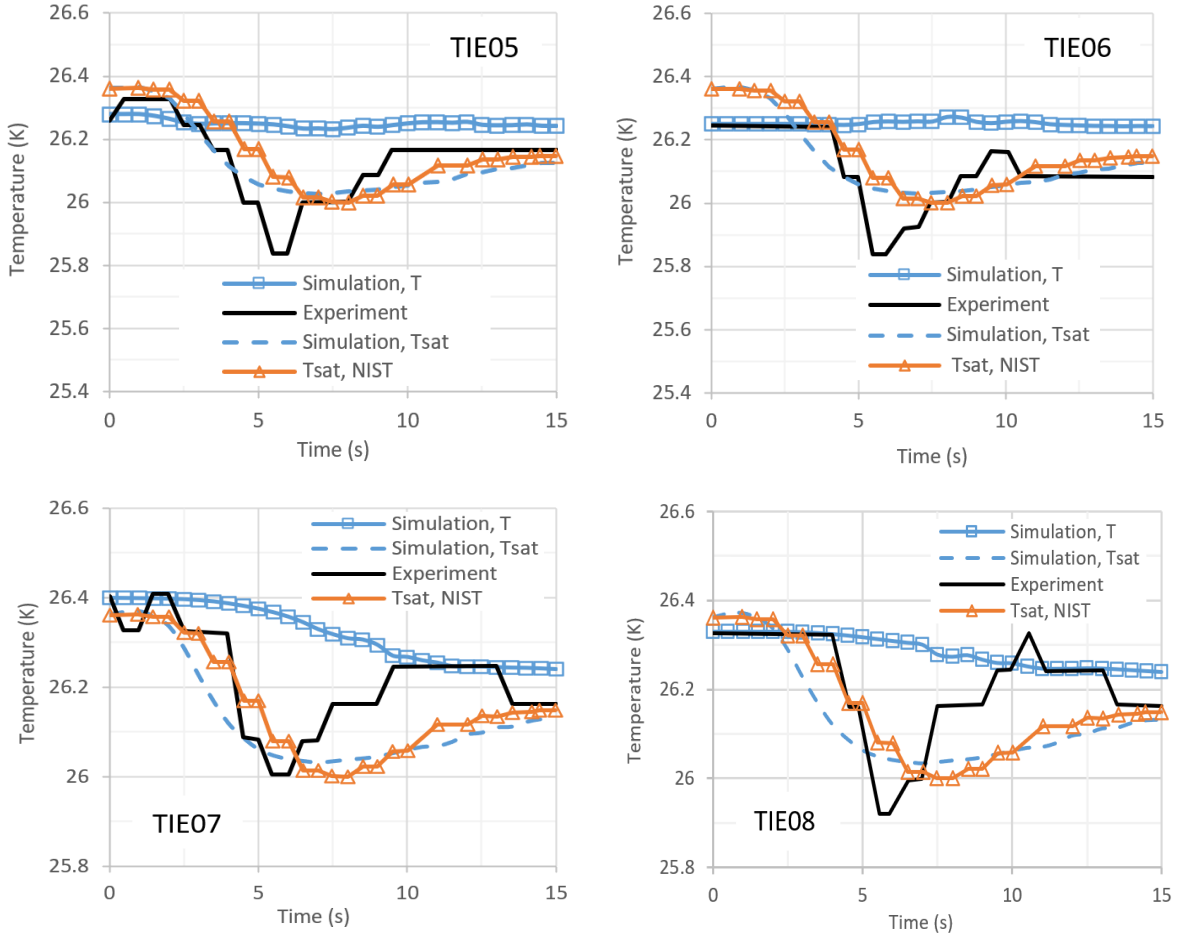


Figure 5. Experimental and simulated LH2 phase temperature dynamics

The authors believe that the difference between experimental and simulated boiling intensity indeed could be explained by the presence of physical thermocouples, which served as “boiling chips” in the experiment, and the absence of such “boiling chips” in the CFD model. Very similar experimental and simulated temperature behaviours are observed for thermocouples TIE06, TIE07 and TIE08. It is observed that the simulated saturation temperatures (T_{sat}) and experimental saturation temperatures determined using NIST database ($T_{sat, NIST}$) are in a close agreement. At the end of the recovery process, the difference between the experimental and simulated LH2 phase temperatures is within 0.1 K for the thermocouples TIE05, TIE07 and TIE08; for the thermocouple TIE06 (height of 5.922 m) the temperature difference is of the order 0.2 K.

Figure 6 shows comparison of the simulated saturation temperatures (“Simulation, T_{sat} ”) with the saturation temperatures corresponding to the experimental pressure (“ $T_{sat, NIST}$ ”) for Lee’s model coefficients $r = 0.05$ (Fig. 6a) and $r = 0.10$ (Fig. 6b) for different thermocouple locations. The model coefficient $r = 0.10$ corresponds to a less favourable agreement between the experimental and simulated saturation temperatures, which is directly connected to the less favourable agreement between the experimental and simulated overpressure dynamics obtained with this coefficient value, as can be seen in Fig. 3. Saturation temperatures obtained with the same coefficient but for different thermocouple locations are practically equal. This is due to the fact that LH2 hydrostatic head provides a negligible contribution to the liquid phase overpressure, which is dominated by overpressure in GH2 phase, therefore resulting in nearly uniform boiling through the entire LH2 phase depth.

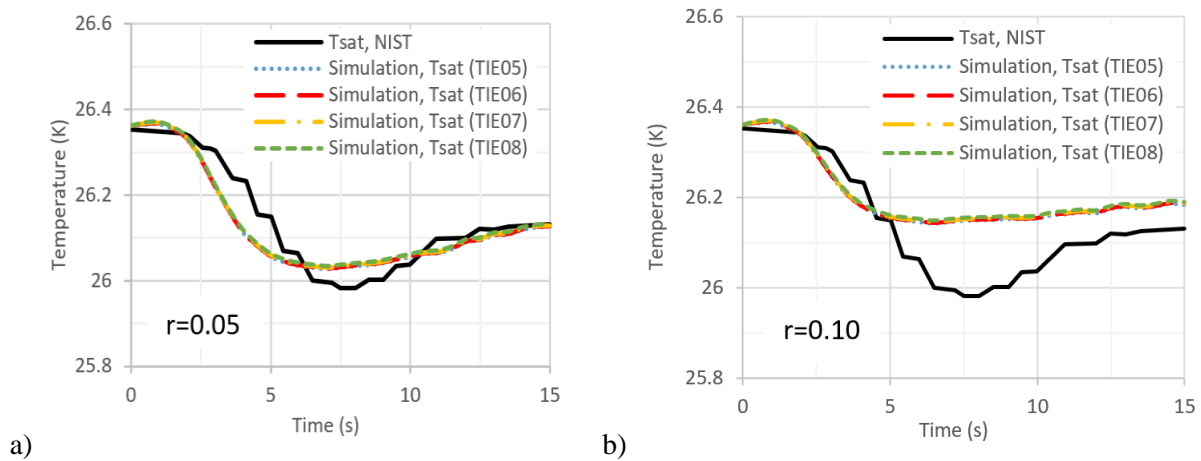


Figure 6. Saturation temperatures at probes TIE05-TIE08 from NIST database and simulated with different Lee's model coefficients: a) $r=0.05$, b) $r=0.10$

5.4 LH2 level dynamics

Figure 7 shows the simulated LH2 level from the initial moment until $t = 15$ s. LH2 level starts to grow ("LH2 swelling") at about $t = 4$ s, reaching its maximum value at $t = 10$ s, which corresponds to the highest intensity of LH2 boiling. In Fig.7, the LH2 highest level is occurred in the simulation at about 3.0 s later than the time of reaching the minimum simulated pressure at $t = 7.0$ s, presented in Fig. 3. The figure also indicates the initial LH2 level (6.248 m) and the location of the protruding vent pipe intake (6.672 m). From Figure 7, it is evident that LH2 does not reach the vent pipe intake during the entire simulated period of 15 s. Additionally, LH2 does not enter the vent pipe even in the process of LH2 "swelling" during the flash-boiling.

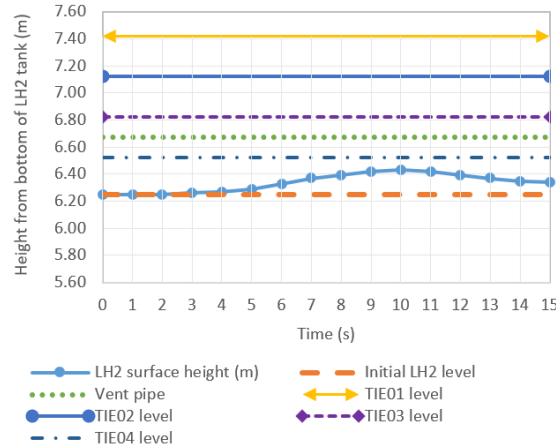


Figure 7. LH2 level dynamics compared to its initial level (6.248 m) and location of the protruding vent pipe intake (6.672 m).

Figure 8 presents the simulated LH2 volume fraction through time. Though the liquid level starts to increase at $t = 4$ s as observed in Figure 7, which indicates start of the boiling, the visible bubbles start to appear at $t = 7.0$ s, as presented in Fig. 8b, when the pressure in the tank reaches minimum level (around 291 kPa). This is consistent as the flash-boiling intensity grows not instantaneously but with a finite speed. As a result, the most intensive boiling and, accordingly, the highest LH2 level occur at $t = 10$ s, when the pressure recovery already started to take place, see Fig. 8c. At $t = 15$ s the pressure is recovered to the value 302 kPa, the saturation pressure grew up and the boiling intensity substantially decreased, shown in Fig. 8d investigated by a reduction of GH2 bubbles generated in the depth of LH2 phase.

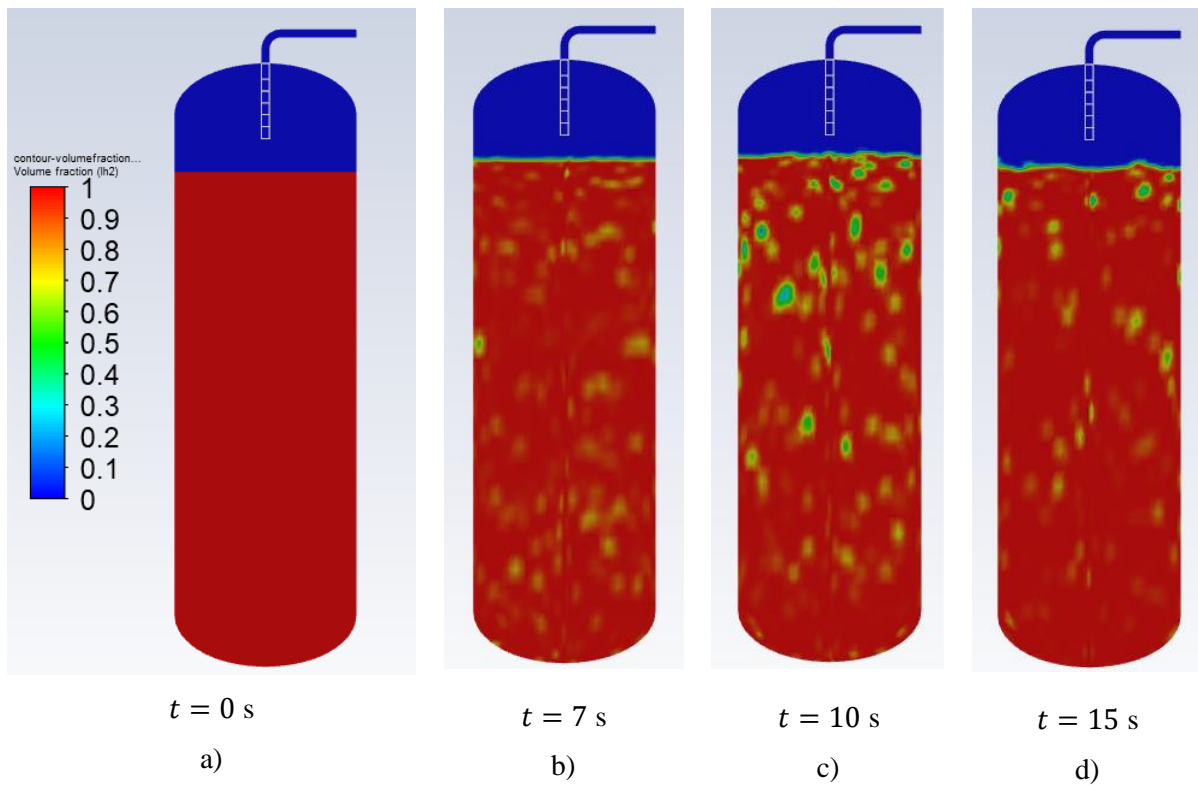


Figure 8. Simulated LH2 volume fraction at different times.

6.0 CONCLUSIONS

A CFD model to predict pressure, temperature and liquid level inside liquid hydrogen storage tank is presented and successfully used to simulate the liquid hydrogen flash-boiling in a pressurised tank during tank's venting process. The model is based on the volume-of-fluid method coupled with Lee's model for evaporation and condensation processes, in which the nature of the Lee's model requires the evaporation and condensation coefficients to be set as empirical coefficients suitable for individually specific problem [22]. The paper originality is in addressing liquid hydrogen behaviour during venting process with the specified mass flow rate, including a detailed study and the explanation of pressure recovery phenomena in LH2 tank during the initial stage of hydrogen flash-boiling process.

The CFD results were compared against the available experimental data from publication [9]. There were rigorously attempts, performed through CFD simulations in order to reproduce the experimental data for pressure recovery:

- Pressure recovery was reproduced during the period of first 15 s of boiling process, applying Lee's model coefficient $r=0.05 \text{ s}^{-1}$;
- The simulated gaseous hydrogen temperatures in ullage closely followed the experimental observations. The difference between experimental and simulated temperature dynamics close to liquid surface was observed, thought to be due to complexity of phenomena close to the interface between liquid and gaseous phase;
- The simulated liquid phase temperature dynamics produced systematic deviation from the experimental observations during the pressure recovery process. The phenomena, explained by non-uniform boiling intensity around thermocouples, was analysed, and supported by a close agreement between the simulated saturation temperature and the saturation temperature determined from experimental pressure dynamics fitted to NIST database. The simulated liquid hydrogen temperatures at the end of the pressure recovery period are close to the experimentally observed ones.

The significance of this study is in the application of the presented multi-phase CFD model for the simulation of the flash-boiling behaviour of liquid hydrogen, the detailed analysis of pressure, temperature, liquid level dynamics due to phase change and tank venting. The pressure recovery process is captured in the simulation, describing the initial pressure drop, then followed by the pressure recovery during the initial stage of the considered liquid hydrogen boiling experiment.

ACKNOWLEDGEMENTS

This research has received funding from the Clean Hydrogen Partnership under grant agreement No. 101101381 (ELVHYS). The project is supported by the Clean Hydrogen Partnership and its members. UK participants in Horizon Europe Project ELVHYS are supported by UKRI grant No.10063519 (University of Ulster) and No.10070592 (Health and Safety Executive).

DISCLAIMER

Funded by the European Union. Views and opinions expressed are however those of the authors only and do not necessarily reflect those of the European Union or the Clean Hydrogen Partnership. Neither the European Union nor the Clean Hydrogen Partnership can be held responsible for them.

REFERENCES

1. Hirt, C.W., Nichols, B.D., Volume of Fluid (VOF) method for the dynamics of free boundaries, *J. Comput. Phys.*, **39**, 1981, pp. 201 – 225.
2. Lee, W.H., Pressure iteration scheme for two-phase flow modeling, *Journal in Multiphase Transport: Fundamentals, Reactor Safety, Applications*, 1980, pp. 407-432.
3. Kim, Y., Choi, J., Kim, S., Zhang, Y., Effects of mass transfer time relaxation parameters on condensation in a thermosyphon, *Journal of Mechanical Science and Technology*, Volume **29**, 2015, pp. 497–5505.
4. Ma, Y., Li, Y., Zhu, K., Wang, Y., Wang, Y., Tan, H., Investigation on no-vent filling process of liquid hydrogen tank under microgravity condition, *International Journal of Hydrogen Energy*, Volume **42**, Issue 12, 2017, pp. 8264-8277.
5. Liu, Z., Li, Y., Zhou, G., Study on thermal stratification in liquid hydrogen tank under different gravity levels, *International Journal of Hydrogen Energy*, Volume **43**, Issue 19, 2018, pp. 9369-9378.
6. Li, J., Liang, G., Zhu, P., Wang, X., Numerical investigation of the operating process of the liquid hydrogen tank under gaseous hydrogen pressurization, *Aerospace Science and Technology*, **93**, 2019, pp. 105327.
7. Zhou, R., Zhu, W., Hu, Z., Wang, S., Xie, H., Zhang, X., Simulations on effects of rated ullage pressure on the evaporation rate of liquid hydrogen tank, *International Journal of Heat and Mass Transfer*, Volume **134**, May 2019, pp. 842-851.
8. Lv, R., Huang, Y., Wu, J., Thermodynamic analysis of partially filled hydrogen tanks in a wide scale range, *Applied Thermal Engineering*, Volume **193**, 2021, 117007.
9. Tani, K., Himeno, T., Sakuma, Y., Watanabe, T., Kobayashi, H., Toge, T., Unno, S., Kamiya, S., Muragishi, O., Kanbe, K., Pressure recovery during pressure reduction experiment with large-scale liquid hydrogen tank, *International Journal of Hydrogen Energy*, Volume **46**, Issue 57, 2021, pp. 29583-29596.
10. Tani, K. , Himeno, T. , Watanabe, T., Kobayashi, H., Toge, T., Unno, S., Kamiya, S., Muragishi, O., Kanbe, K., CFD simulation of pressure reduction inside large-scale liquefied hydrogen tank, International Confererence on Hydrogen Safety (ICHs), 2021.
11. Kassemi, M., Kartuzova, O., Effect of interfacial turbulence and accommodation coefficient on CFD predictions of pressurization and pressure control in cryogenic storage tank, *Cryogenics*, **74**, 2016, pp. 138–153.
12. Stochl, R.J., Maloy, J.E., Masters, P.A., et al., Gaseous-Hydrogen Requirements for the Discharge of Liquid Hydrogen From a 1.52-Meter-(5-FT) Diameter Spherical Tank, NASA Technical Note, D-5336, 1969.

13. Watanabe, T., Nakano, A., Kambara, K., Tokunaga, K., Shiigi, T., Shimojima, K., Phenomena of liquid nitrogen flashing under rapid depressurizations, *International Journal of Multiphysics*, Volume **16**, Number 3, 2022, pp. 223 - 233.
14. Molkov, V., Shentsov, V., Numerical and physical requirements to simulation of gas release and dispersion in an enclosure with one vent, *International Journal of Hydrogen Energy*, Volume **39**, Issue 25, 2014, pp. 13328-13345.
15. Smagorinsky, J., General circulation experiments with the primitive equations. I. The Basic Experiment. *Month. Wea. Rev.*, **91**, 1963, pp. 99-164.
16. Prakash, C., Two phase model for binary liquid-solid phase change: Part I and II, *Numerical Heat Transfer*, **18**, 2, 1990, pp. 131 – 167.
17. Peng, D.Y., Robinson, D.B., A new two-constant equation of state, *Ind. Eng. Chem., Fundam.*, Vol. **15**, No. 1, 1976, pp. 59 – 64.
18. NIST Chemistry Webbook, NIST Standard Reference Database Number 69, available at <https://webbook.nist.gov/chemistry/>
19. Leachman, J.W., Jacobsen, R.T., Penoncello, S.G., Lemmon, E.W., Fundamental equations of state for parahydrogen, normal hydrogen, and orthohydrogen, *J. Phys. Chem. Ref. Data*, Vol. **38**, No. 3, 2009.
20. McCarty, R.D., Hord, J., Order, H.M., Selected properties of hydrogen (engineering design data), Technical Report, U.S. Department of Commerce/National Bureau of Standards Monograph 168, 1981.
21. Stewart, M., Moder, J.P., Self-pressurization of a flightweight, liquid hydrogen tank: simulation and comparison with experiments, AIAA 2016-4674, 52nd AIAA/SAE/ASEE Joint Propulsion Conference, July 2016.
22. Kharangate, C.R., Mudawar, I., Review of computational studies on boiling and condensation, *International Journal of Heat and Mass Transfer*, Volume **108**, Part A, 2017, pp. 1164 - 1196.